A Novel Pattern Recognition Method for Self-Powered TENG Sensor Embedded to the Robotic Hand

by

Azat Balapan

Submitted to the Department of Robotics and Mechatronics
in partial fulfillment of the requirements for the degree of

Master of Science in Robotics

at the

NAZARBAYEV UNIVERSITY

Apr 2025

Author .....
Department of Robotics and Mechatronics
Apr 29, 2025

Certified by .....
Atakan Varol and Azamat Yeshmukhametov
Associate Professors
Thesis Supervisor

Accepted by .....
Elizabeth Arkhangelsky
Dean, School of Engineering and Digital Sciences

A Novel Pattern Recognition Method for Self-Powered TENG Sensor Embedded to the Robotic Hand

by

Azat Balapan

Submitted to the Department of Robotics and Mechatronics
on Apr 29, 2025, in partial fulfillment of the
requirements for the degree of
Master of Science in Robotics

Abstract

This paper details the design and validation of a robotic hand resembling human anatomy, featuring triboelectric nanogenerator (TENG) sensors for enhanced shape and material identification. In contrast to conventional piezoelectric sensors—often susceptible to temperature shifts and high production expenses—TENGs offer a self-sustaining power source, simplified circuitry, economical fabrication, and robust durability. Leveraging these advantages, this work introduces a novel machine learning framework that converts sequential TENG sensor data into two-dimensional representations, subsequently analyzed by a 2D convolutional neural network (CNN). Comparative studies with a standard 1D CNN approach reveal marked improvements in performance: the 2D CNN model achieves classification accuracies of 98% for shape recognition and 99% for material discrimination, surpassing the respective 94% and 98% attained via 1D CNN. Integral to this methodology are TENG sensor fabrication, noise suppression measures, a custom robotic hand design, and associated control electronics. Real-time tests confirm the proposed system's resilience and adaptability in unstructured environments, highlighting the promising role of integrating TENG sensors with advanced neural network architectures for autonomous, dexterous manipulation across a range of industrial applications.

Thesis Supervisor: Atakan Varol and Azamat Yeshmukhametov
Title: Associate Professors

Acknowledgments

This research received funding under project number AP23486880 from the Ministry of Higher Education and Science of the Republic of Kazakhstan, as well as project numbers 111024CRP2010 and 20122022FD4135 from Nazarbayev University.

Contents

List of Figures

List of Tables

Chapter 1

Introduction

The pursuit of more sophisticated robotic hands hinges upon the creation of tactile sensors capable of accurately identifying both shapes and materials. Within the spectrum of sensor technologies, triboelectric nanogenerators (TENGs) have emerged as a promising substitute for conventional piezoelectric sensors, primarily due to their inherent ability to self-power [5, 29, 56, 20, 59], cost-efficient manufacturing process [21], and heightened durability [54, 1]. These merits make TENGs highly appealing for applications in autonomous robotics, including hands that emulate human dexterity.

Despite the effectiveness of traditional piezoelectric sensors, they exhibit certain drawbacks such as heightened sensitivity to ambient temperature changes and elevated production expenses. Conversely, TENGs utilize the triboelectric principle to transform mechanical motions into electrical signals [5], offering a rugged and economical sensor alternative. Their integration into robotic platforms can substantially elevate a system's capability to perceive and respond to physical contacts. Foundational studies pioneered by Wang have underlined TENGs' versatility and their viability across various practical domains [50, 32, 51].

When used for classification tasks, conventional machine learning methods employing TENG-based tactile sensors often reach accuracy levels starting around 91% [37, 38]. These traditional approaches commonly employ one-dimensional convolutional neural networks (1D CNNs) [28, 44, 46, 48] to handle sequential data, thereby capturing temporal patterns within the signals. Nonetheless, it has also been reported

that classification accuracy with 1D signal processing can be as low as 82% in certain TENG sensor-based applications [17]. Moreover, while 1D CNNs excel in extracting temporal features, they may not fully leverage the inherent spatial structures in sensor data [6, 47, 14]. Indeed, studies indicate that 2D CNNs generally achieve superior accuracy [52], though the adoption of higher-dimensional models—such as 3D LSTM networks—can yield classification rates of 94.1% to 99.2% [62], albeit at the cost of increased data requirements and computational demands.

To tackle these challenges, this work introduces a novel strategy that converts time-series TENG data into two-dimensional representations (images), subsequently analyzed by 2D CNNs. By capturing spatial hierarchies in addition to temporal characteristics, these 2D CNNs can potentially offer more robust and accurate shape and material classification. Previous research has demonstrated that 2D CNNs exhibit exceptional performance in diverse image-processing tasks [15, 34, 43, 39, 42], underscoring their suitability for applications involving image-based data [15].

Deep learning approaches such as CNNs have transformed numerous fields, including computer vision and industrial fault detection [15, 34], largely because of their ability to capture multi-level feature representations [60, 22]. Within the mechanical domain, for example, 2D CNNs have proven adept at fault diagnosis in rotating machinery [10], reinforcing the argument that they can effectively model complex spatial dependencies.

By uniting TENG sensors with these advanced neural architectures, the resulting tactile sensing platform gains significant reliability and precision—qualities crucial for robotic manipulation. Accordingly, this paper expands upon prior breakthroughs in TENG sensor development and CNN-based data processing, focusing particularly on leveraging 2D image transformations of sensor signals for enhanced recognition.

The presented research offers a design for a human-inspired robotic hand outfitted with TENG sensors, achieving marked improvements in shape and material detection. While various studies have validated TENG sensors in tactile systems and CNN-based methods in pattern recognition, few endeavors have integrated two-dimensional data representations for TENG signals to further boost accuracy and

resilience. By proposing and validating this image-centric interpretation of sensor outputs, the work establishes new performance baselines for TENG-driven tactile systems in robotics. Experimental comparisons between the standard (one-dimensional) and proposed (two-dimensional) approaches highlight the higher effectiveness of the latter in classification tasks. Detailed descriptions are provided for TENG fabrication steps, noise-suppression techniques, hardware design of the robotic hand, and control electronics implementation. Ultimately, the results illustrate the method's robustness in challenging environments, emphasizing the advantages of combining TENGs with advanced 2D CNNs for a variety of industrial use cases.

Chapter 2

Literature review

In the field of robotics, there are many devices to explore the environment in terms of temperature, pressure or any other characteristics that humankind could sense or perceive. The perception of touch is commonly referred to as the concept of haptics or haptic touch [3]. Human haptics is one of the directions in which robotics work on simulating the same sense for the robots. For this purpose, researchers have developed tactile sensors.

2.1 Piezoelectric sensors

2.1.1 Piezoelectricity and piezoelectric effect

The term "Piezoelectricity" originated in 1880 and was discovered by French scientists Pierre and Jacques Curie [41, 9, 45, 36, 33]. This effect, also known as piezoelectric effect or polarization, describes the generation of electricity due to mechanical stress applied to the substance [41, 9, 45, 4]. There also exists "piezo resistance" and "piezo capacitance" that result from change in electrical resistance and capacitance of the substances respectively due to mechanical stress [41, 9, 45]. The substance of interest for piezoelectricity is a material with its crystal internal structure [3, 41, 9, 45, 36, 4]. Here it should be specified what "crystal internal structure" means. All environments around us consist of tiny particles called atoms. Atoms are building blocks

of molecules and molecules are bonding in something bigger and so on. Crystalline internal structure means that molecules appear in forms of crystal (see Figure 2-1).

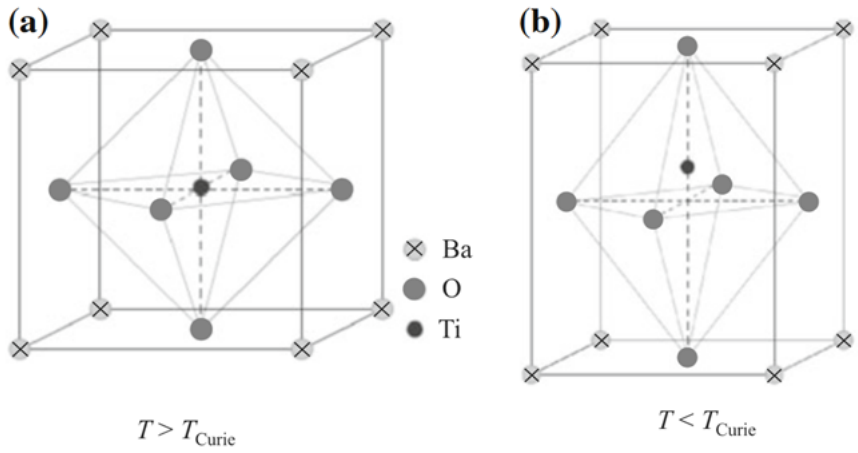

Figure 2-1: Crystal structure of piezoelectric ceramic at different temperatures [9].

As it was mentioned, piezoelectric effect causes electricity and there is a need to calculate the amount of generated electricity. The earliest attempt (in 1922) of mathematical approval of calculating the amount of power (polarization) generated from piezoelectricity considered the ground method of the concept and analyzed the applied stress to the material [4, 45]. In 1972, Martin Richard wanted to challenge this method by introducing new parameters of electric charges into the equation [35]. The term "uniform strain" in his work [35] appears in the more recent book published in 2017 [45] meaning that the mathematical model described by Martin is consistent. Even though mathematical models describe any phenomenon with good precision and accuracy, in practical sense, the question stands whether it is efficient to apply pre-established mathematical models. It should be mentioned that the first complete device named "oscilloscope" which was able to sense any voltage in real time was invented in early 1920s [7]. And ever since, it became a handful device for measuring the amount of any electricity or in our case polarization. Later, in this work it will be clearly seen that in experiments, practically, researchers rely more on such devices rather than calculating mathematical models.

2.1.2 Piezoelectric materials

As for now, piezoelectric materials are those that appear as crystals in their internal structure and those that provide electricity due to application of the stress on them. It was stated that one of such ceramics is made from lead titanate ($PbTiO_3$) and it has a second name of PZT polymer [41, 9, 45]. It is a common practice to manufacture a tactile sensor from PZT polymer and analyze how much voltage it will generate due to applied force [25, 19, 2]. In some specific cases [25], research refers to the historical mathematical model [4] to provide general information on theoretical principles. Nonetheless, output voltage analysis of PZT sensors performed by researchers is conducted via measurement tools [25, 19, 2]. It was stated that by application of force about 0.12 N in magnitude, PZT tactile sensors could generate either 28 mV [19] or 600 mV [2] depending on the materials used in the sensor manufacturing process. For better understanding of these results let's compare them with other types of materials used for piezoelectric sensors.

Another material which experiences a piezoelectric effect was discovered in 1969 by Kawai and it was made from polyvinylidene difluoride (PVDF) [9, 45]. One of the early attempts in building a tactile sensor from PVDF was performed in 1995 by Edward et al. [24]. In their experiment, they used several pieces of PVDF sensors and arranged them in matrix form to see the output of each [24] (see Figure 2-2). This procedure of making tactile sensors by arranging sensors in matrix form was duplicated in much more recent works [25, 31, 57]. A logical consideration of Figure 2-2 gives an idea of the working principle of the piezoelectric PVDF tactile sensors. It is obvious that combination of each output in the matrix will give an approximate shape of the object which is placed on top of the sensor. The question is about the efficiency of such tactile sensors.

The response of the PVDF sensors with application of the 0.12 N could vary with approximate values of 7.5 V [8], 60 V [23], 30 V [27]. These results are much higher and better than those obtained from PZT sensors [19, 2]. Nonetheless, are there any better types of tactile sensors with either greater voltage generation or with a more

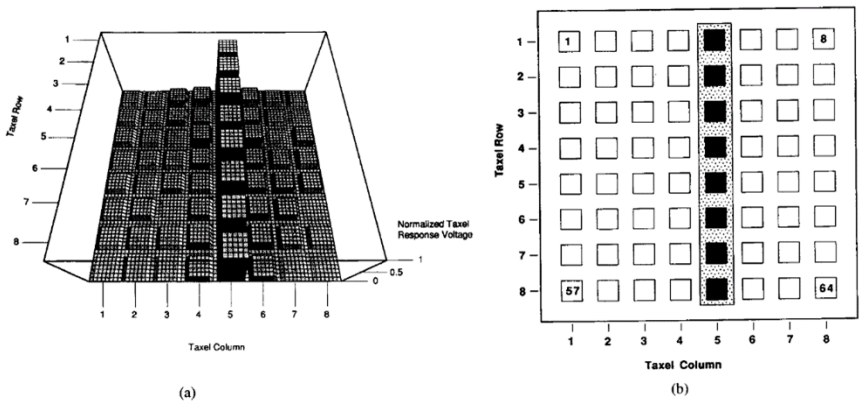

Figure 2-2: (a) Voltage response of each PVDF sensor in 3D plot. (b) Arrangement of the PVDF sensors from top [24].

effective structure so that there is no need to arrange tactile material in matrix form?

2.2 Triboelectric sensors

2.2.1 Triboelectricity and triboelectric effect

If one puts the words "triboelectricity" or "triboelectric effect" into academic search engines, the majority of appeared literature will be in form of review papers. This leads to the conclusion that there exist more applications of such an effect rather than definitions of the terms. One of the works which tried to give the definition of the triboelectric effect was written by Cheng Xu et al. in 2018 [53]. They studied the concept of two oppositely (positively and negatively) charged materials producing electricity due to physical contact among them by citing the most accepted physical concepts like Maxwell's equation [53]. Nonetheless, this concept is used in older works for fabrication of triboelectric nanogenerators under names of "TEG" [11] or "TENG" [**?**]. The powerful schematics of the working principle was given by one of them [11] (see Figure 2-3).

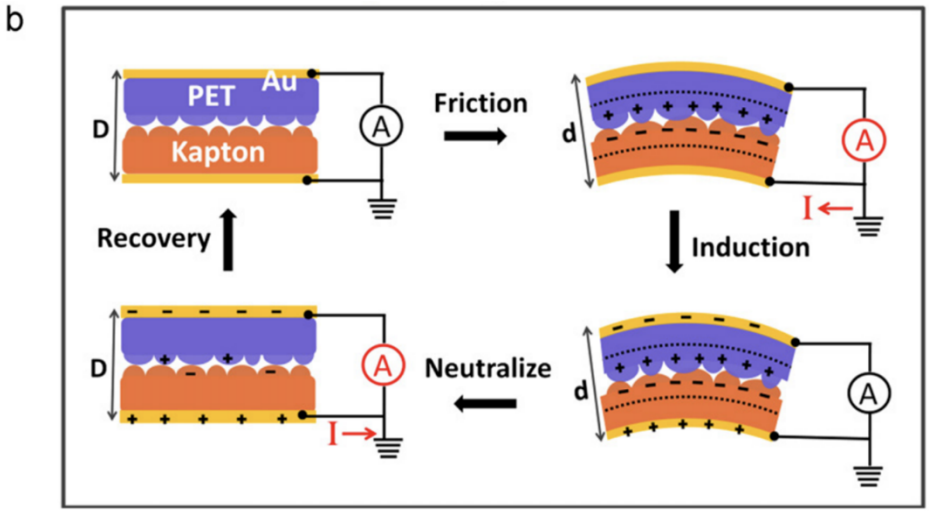

Figure 2-3: Working principle of TEG [11].

2.2.2 Triboelectric materials

In fabrication of triboelectric nanogenerators researchers used either polyvinyl chloride (PVC) [11, 61] or polydimethylsiloxane (PDMS) [**?**, 55, 40]. Interestingly, most of these works used capacitors to accumulate energy in their experiments [11, 61, 55, 40]. From globally accepted physics, capacitors are energy storing elements meaning that TENG sensors are able not only to generate tactile feedback, but also to generate excessive electricity that could be stored. For example, if one continuously taps the TENG sensor every 2 seconds for 160 seconds, the accumulated 4.5 V of electricity in a capacitor could keep an electronic watch alive for 15 seconds [40], while others argue that this electronic watch could work for 25 seconds if constant tapping lasts for 200 seconds [55]. Furthermore, in comparison with conventional PVDF and PZT piezoelectric sensors [19, 2, 8, 23, 27], despite the fact that the output was calculated using the same method of application of some force applied to both PVC and PDMS TENG sensors, the main characteristic which defined output voltage was frequency [11, **?**, 61, 55, 40]. Moreover, it is stated that the output voltage is dependent on pressure only if it exceeded 70 000 Pa of pressure [40]. The last two facts lead to the idea that TENG sensors are more efficient than piezoelectric sensors if the application requires a repetitive task where the frequency of repetition is more important than

the force exerted on a tactile sensor.

2.3 TENG Sensor Fundamentals

The triboelectric effect, an electrostatic phenomenon that arises when two materials with contrasting electron affinities come into repeated contact, underpins TENG functionality [49]. This charge exchange manifests as measurable electrical signals, allowing TENG sensors to act both as energy harvesters and sensing elements [16]. In robotics, TENGs can be molded to fit curved surfaces, such as finger phalanges, making them well-suited for capturing tactile information in real time [30].

Initially, TENG-based sensor designs focused on verifying fundamental performance metrics like output voltage range, response time, and cycle durability [26]. Progressively, researchers have begun to explore more advanced functionalities, such as dynamic pressure mapping for object shape detection [12]. Emerging patterns suggest that triboelectric signals inherently contain both temporal and spatial features, which remain underutilized by straightforward threshold-based or 1D signal processing approaches [18, 58].

2.4 Integration into Robotic Hands

Robotic hands often demand flexible, conformable sensors that can be embedded onto multiple phalanx segments without hindering motion or adding excessive weight [13, 30]. TENG sensors excel in such configurations because they do not require constant external power; they harvest small amounts of energy from each contact event [49, 18]. This reduces wiring complexity and can extend the autonomy of a robotic system.

Although TENG sensors are promising, challenges persist:

- **Environmental Sensitivity:** Triboelectric signals can fluctuate due to variations in humidity, temperature, or surface roughness of contacting materials [16].

- **Noise Interference:** Single-electrode TENGs, in particular, are prone to external electromagnetic interference, necessitating noise-cancellation strategies and carefully grounded circuits [13].

- **Calibration Complexity:** Ensuring consistent output across multiple TENG patches requires calibration, especially if each patch has slightly different thicknesses or electroactive areas [12].

2.5 Machine Learning Approaches to TENG Signal Analysis

2.5.1 1D CNNs and Their Limitations

Traditional machine learning frameworks for TENG data typically rely on 1D convolutional neural networks (CNNs) to process time-series signals [49, 58]. By convolving filters over time, 1D CNNs capture local temporal patterns, which can yield high accuracy in controlled conditions [16]. For instance, some studies have reported classification accuracies exceeding 90% for shape or surface recognition tasks [26, 30].

However, 1D CNNs often overlook spatial relationships—especially relevant if multiple TENG patches form an array across a robotic hand [13, 18]. Simply concatenating data from multiple sensors into a single sequence may discard valuable information about where on the hand the contact occurred. As a result, classification rates can drop in more complex scenarios, such as identifying diverse objects under varying forces or angles of contact [12].

2.5.2 2D CNNs and Image-Based Representations

To address these deficiencies, numerous studies have transitioned toward **2D CNNs**, converting time-sequential sensor outputs into image-like matrices [18, 58]. Each row (or column) of this matrix could correspond to a specific TENG sensor at a particular time step, creating a grid that preserves spatial ordering across sensors [16]. This

approach benefits from techniques honed in computer vision, where 2D convolutions excel at discovering spatial hierarchies.

Recent work has demonstrated that 2D CNNs can achieve accuracy gains of up to 5–10% compared to their 1D counterparts in tasks like multi-object recognition or material identification [26, 30]. Besides improved accuracy, image-based methods also foster data augmentation strategies—e.g., rotating or shifting the matrices—to artificially expand the dataset, further enhancing model robustness [58].

2.5.3 Beyond 2D: LSTMs and 3D CNNs

While **2D CNNs** provide a balance between model complexity and performance, a few studies are exploring LSTM (Long Short-Term Memory) layers or **3D CNNs** to model deeper spatiotemporal features [13, 18]. These advanced architectures can yield classification rates surpassing 95%, yet they often demand larger training datasets and more extensive computational resources—conditions not always feasible for real-time robotic control [12].

2.6 Noise Cancellation and Hardware Considerations

Recognizing the influence of external interference on TENG signals, recent research efforts have emphasized **noise cancellation** techniques [26, 13]. Shielding sensor leads, grounding all unused input pins, and implementing differential measurement setups can greatly mitigate interference [16]. When combined with software-level filtering—such as wavelet denoising or threshold-based segmentation—TENG signals become more reliable for downstream machine learning models [18].

Hardware improvements also factor into these solutions. Advancements in flexible electrodes and optimized polymer–metal layer designs have reduced sensor drift and susceptibility to mechanical fatigue [12]. Meanwhile, calibrating each sensor pad under varying force levels ensures consistent voltage outputs, enabling robust cross-comparisons among different TENG patches on the same robotic hand [16].

2.7 Research Gap and Proposed Direction

Despite progressive strides, large-scale deployments of TENG sensors in robotic hands remain in early stages. Existing methods typically present high performance in **controlled** laboratory settings, yet show vulnerability in **real-world environments** (temperature fluctuations, dusty conditions, or inconsistent contact angles) [49, 58]. Moreover, bridging the gap between 1D and 2D data processing offers a tangible path to enhance classification accuracy without incurring the resource overhead of 3D networks [13].

This work proposes a strategy combining **TENG sensor arrays**, **hardware-based noise reduction**, and **2D CNN** frameworks, building on the literature that demonstrates the viability and efficiency of TENG sensors [26, 30, 12]. By focusing on image-based data transformations, the approach aims to capture both temporal dynamics and spatial interrelationships. The outcome is expected to streamline shape and material classification for a robotic hand—facilitating more stable grasping, nuanced manipulation, and overall improved autonomy.

Chapter 3

Research Methodology

This chapter offers a comprehensive explanation of the steps taken to fabricate the TENG sensor and describes, in detail, how the robotic hand was constructed. It then delves into the methodology behind an established machine learning approach and concludes by contrasting that method with the newly proposed technique.

3.1 Preparation of a TENG sensor

Ecoflex® 00–30 (Smooth-On, Inc., USA) served as the polymer foundation for creating the TENG sample. This material has a density of 1.07 g/cc and provides a working time of approximately 45 minutes.

Initially, a rectangular piece was cut from a carbon cloth to dimensions of 16 mm × 50 mm (Fig. 3-1a). Next, a copper wire was sewn through the center line of the cloth using a needle. This procedure enhanced both the electrical connection between wire and cloth and provided insulation for the wire (while also reinforcing the sensor).

After cutting and attaching the wire, the cloth was placed into a 3D-printed polylactic acid (PLA) mold. Both ends of the cloth were pulled taut and held in place by plastic plates to maintain tension. This setup ensured that Ecoflex would evenly coat the carbon cloth on both sides during curing.

To produce the Ecoflex mixture, components A and B were measured at a 1:1 ratio by volume. The mixture was then subjected to vacuum degassing at 25°C to

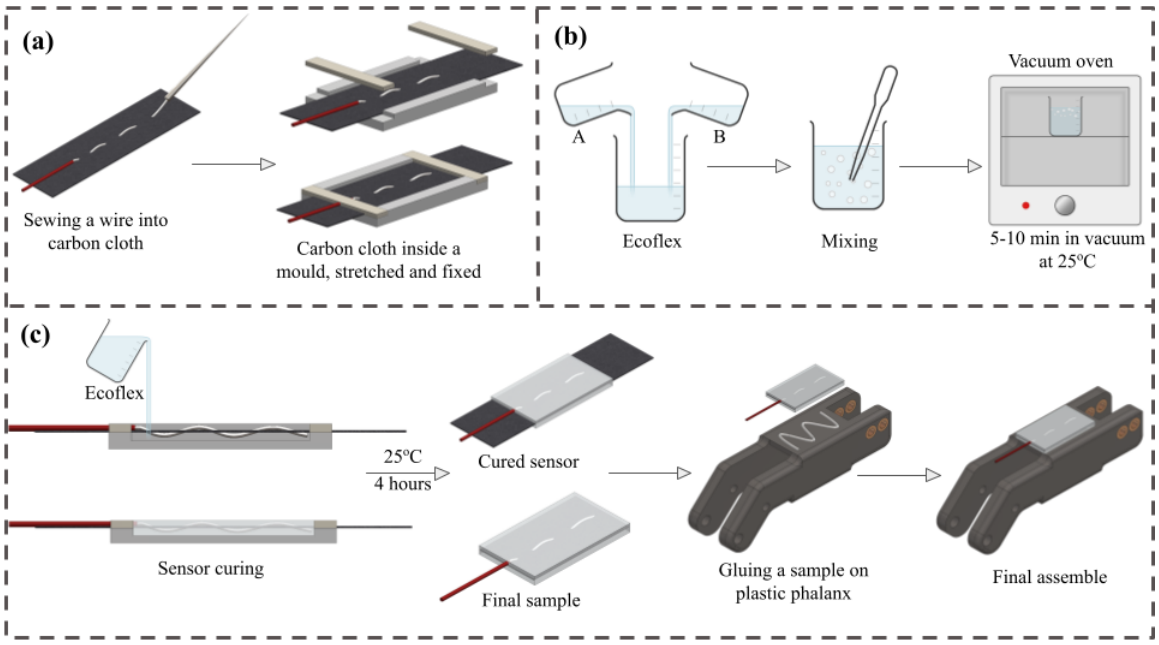

Figure 3-1: TENG sensor preparation

eliminate air bubbles (Fig. 3-1c).

Once degassed, the Ecoflex was poured into the mold containing the taut carbon cloth and allowed to cure for roughly four hours. After curing, surplus carbon cloth was trimmed away, and the sensor was cut to match a specific finger phalanx shape using a surgical blade. Lastly, the sensor was bonded to the top surface of a plastic phalanx using a cyanoacrylate (super glue) adhesive.

3.2 Noise Cancellation

Voltage outputs from the sensors were initially captured using an Arduino Mega 2560. All 12 sensors were connected to the Arduino's analog input pins (Fig. 3-2a). Graph A in Fig. 3-2a presents the acquired data, illustrating that single-electrode TENG sensors are vulnerable to external noise, even when the sensor does not physically contact a surface.

To mitigate these unwanted fluctuations and to generate data more suitable for machine learning applications, a more robust data collection configuration was devised. As shown in Fig. 3-2b, three Arduino Mega 2560 boards were employed. Each

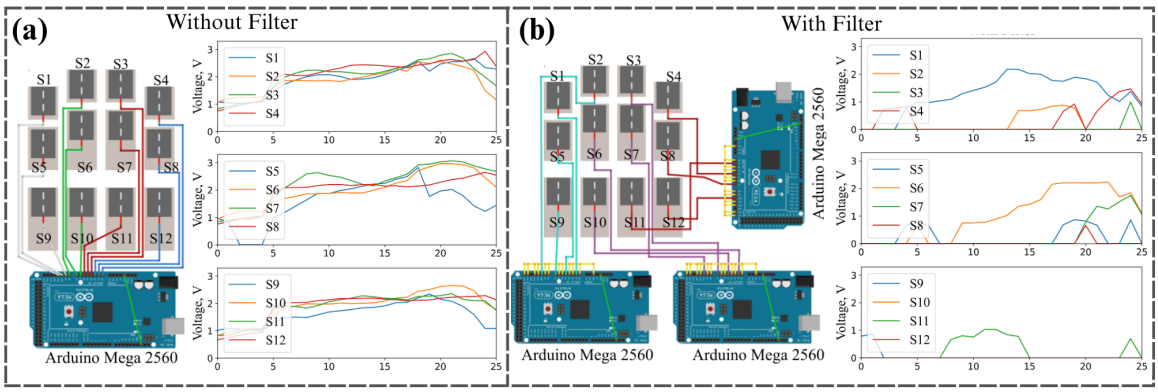

Figure 3-2: Data collection setup without and with noise filtering

board was connected to four sensors via analog pins (labeled A1, A4, A7, and A10), while all unused analog pins were grounded. A script systematically read every analog input pin inside the `void loop`, and subsequently utilized sensor values. This arrangement substantially reduced noise levels, limited interference among neighboring sensors, and allowed the sensors to reliably detect contact with an object's surface (Fig. 3-2b).

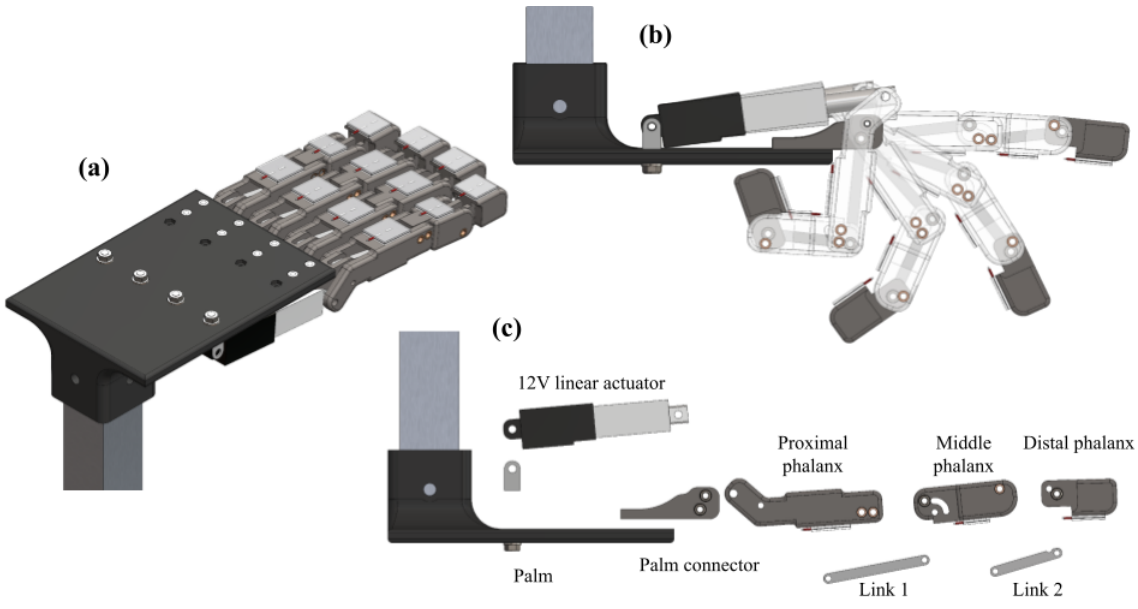

Figure 3-3: CAD design of a robotic hand

3.3 Design and Assembly of the Robotic Hand

The robotic hand shares morphological similarities with the human hand, featuring four fingers (but no thumb). Each finger comprises three phalanges: distal, middle, and proximal, joined by rotational joints (Fig. 3-3c). A 12 V linear actuator (capable of a 200 N load) drives finger movement, as shown in Fig. 3-3b. The actuator exerts force on the proximal phalanx, while a pair of link bars steer the finger through a motion path akin to that of a human digit.

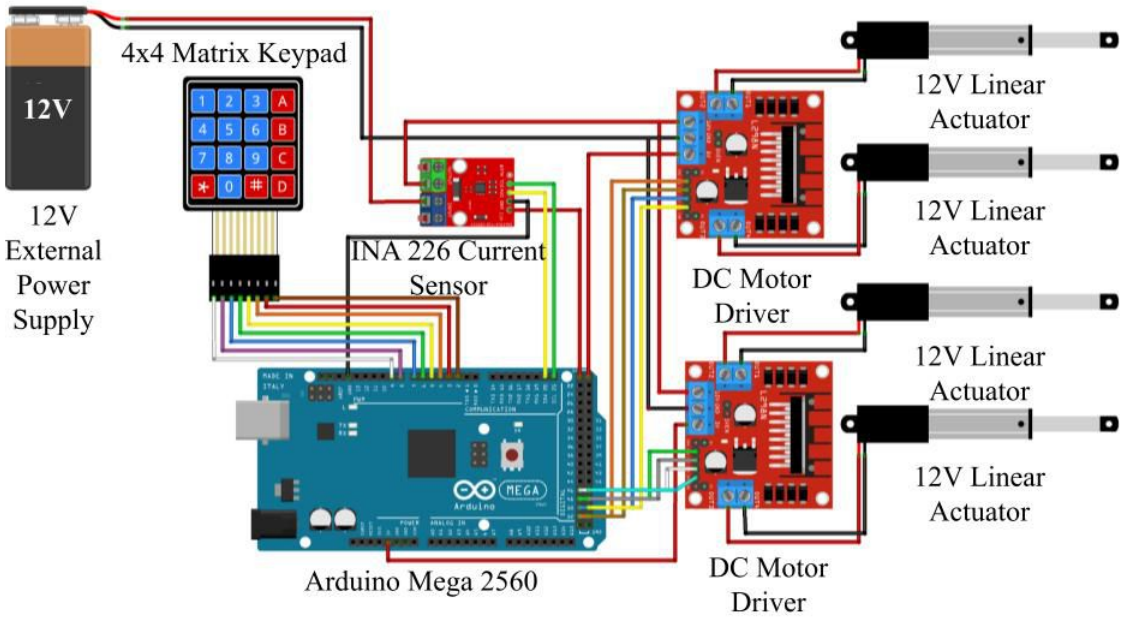

Figure 3-4: Robotic hand electronic schematics

Each TENG sensor is sized to fit a respective phalanx (Fig. 3-3a), with sensors attached on the distal and proximal phalanges of each finger. The middle phalanges on the two central fingers are longer by approximately 10 mm, so the corresponding sensors are made proportionally bigger.

Control signals originate from an Arduino Mega 2560 (see Fig. 3-4), but because the linear actuators require 12 V, separate DC motor drivers handle the higher voltage from an external 12 V supply. An INA 226 current sensor is also included for real-time monitoring of current. When the robotic hand detects that current usage has risen due to contact with an object, the INA 226 feeds back a signal, causing the actuators

to stop and preventing the hand from fully closing against an obstacle.

3.4 Sensor Calibration

To maintain reliable voltage readings, each TENG sensor was calibrated before being mounted on the robotic hand. A set of known forces (0.5 N to 5 N) was applied to the sensor surface using a force gauge. Voltage signals were gathered, averaged, and plotted to establish a force-to-voltage reference curve. This calibration curve was then employed to adjust raw sensor measurements, correcting for initial bias or drift. Additionally, each of the 12 TENG units was tested against a 3.3 V reference voltage to ensure cross-sensor uniformity. This overall calibration approach ensured consistent sensor outputs even when phalanges or sensors were replaced.

3.5 Existing Machine Learning Method: Signal Processing

3.5.1 Data Collection and Preprocessing

After constructing the robotic hand and integrating the TENG sensors, data was gathered for classifying both shapes and materials.

Under the existing method, the TENG-based sensors attached to the robotic hand recorded voltage readings (up to 3.3 V). Each shape's dataset comprised around 160,000 sequential voltage samples. Despite the noise mitigation setup, it was noted that some sensors still recorded a signal in the absence of direct contact with any object. Therefore, a threshold of 1.55 V was selected to distinguish real contact readings from background noise. This step reduced each shape's data to about 31,000 sequential points.

Subsequent segmentation involved grouping each continuous reading into windows of 12 points each. Then, 12 such windows (for a total of 144 data points) were treated as a single batch. Conceptually, these batched signals represent one-dimensional

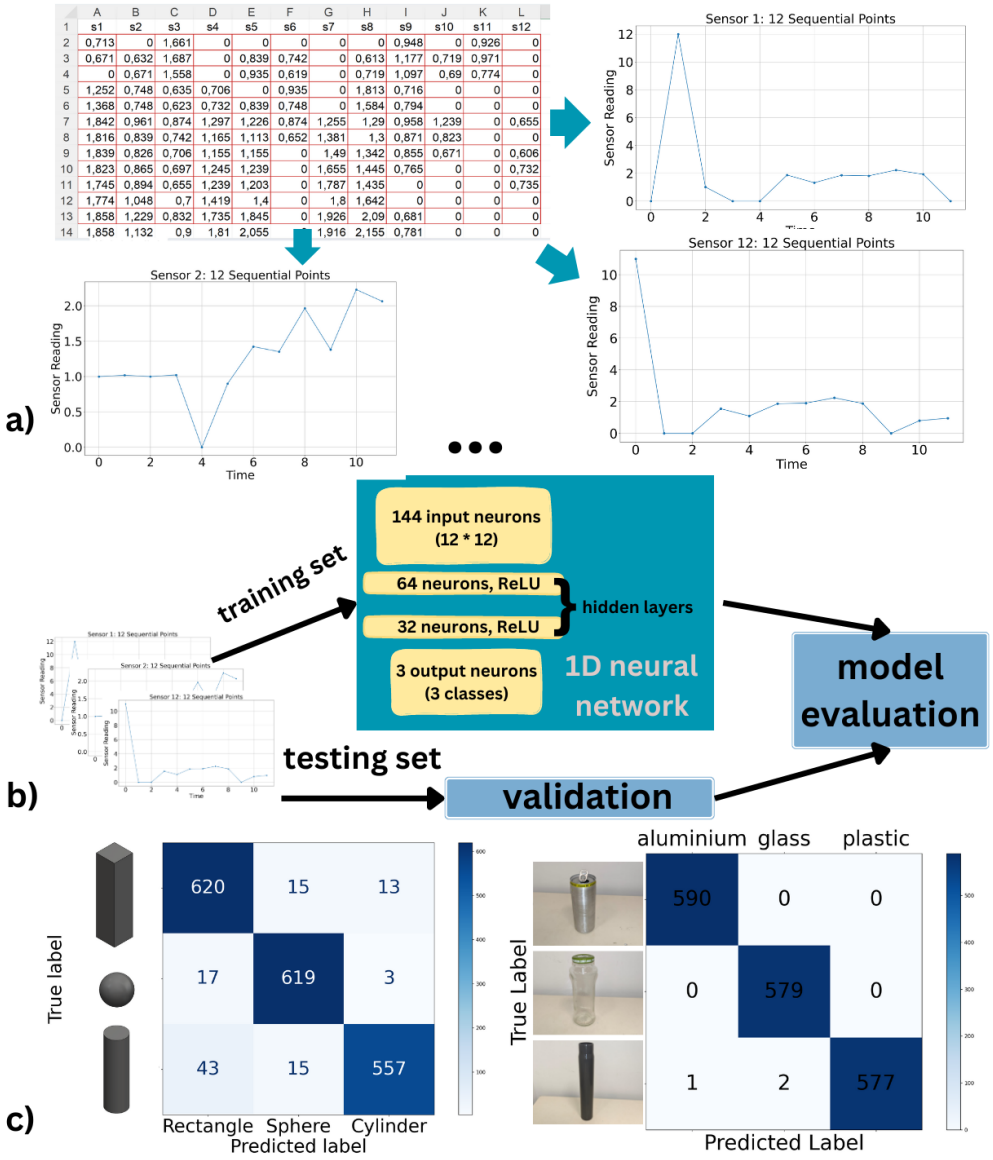

Figure 3-5: (a) Data collection and plotting process. (b) 1D convolutional network architecture. (c) Confusion matrix showing the overall accuracy of the model.

sequences.

Line charts were generated to illustrate normalized voltage intensities for these sensor readings (Fig. 3-5a). This visualization helped expose specific signal patterns tied to each shape, enabling the neural network to differentiate among them.

3.5.2 Model Training and Evaluation

A one-dimensional neural network (1D NN) was deployed for sequential data processing. Its architecture was geared toward capturing temporal relationships within the data (Fig. 3-5b). The optimizer was Adam, and sparse categorical cross-entropy was used as the loss function.

After training, performance was assessed via a confusion matrix (Fig. 3-5c). The accuracy measure was:

$$\text{Accuracy} = \frac{\text{TP}_{\text{cylinder}} + \text{TP}_{\text{rectangle}} + \text{TP}_{\text{sphere}}}{\text{Total number of samples}},$$

where TP denotes the correctly predicted instances for a specific shape. Based on the confusion matrix outcomes, shape classification accuracy reached 94%, whereas material classification attained 99% accuracy.

3.6 Proposed Machine Learning Method: Image Processing

3.6.1 Data Collection and Preprocessing

The proposed approach also collects sensor data from the robotic hand, yet applies the same 1.55 V threshold to limit noise. This filtering yields roughly 31,000 sequential samples for each shape (Fig. 3-6a).

Those sequential readings are then rearranged into 12×12 matrices, representing a brief time window of the voltage signals. Each matrix is translated into a grayscale image, normalized by the maximum voltage (3.3 V), thereby constraining pixel values between 0 and 1.

By visualizing these 12×12 matrices as images, each pixel encapsulates a sensor voltage intensity (Fig. 3-6b). The spatial pattern made evident in these matrices is key for effectively distinguishing different shapes.

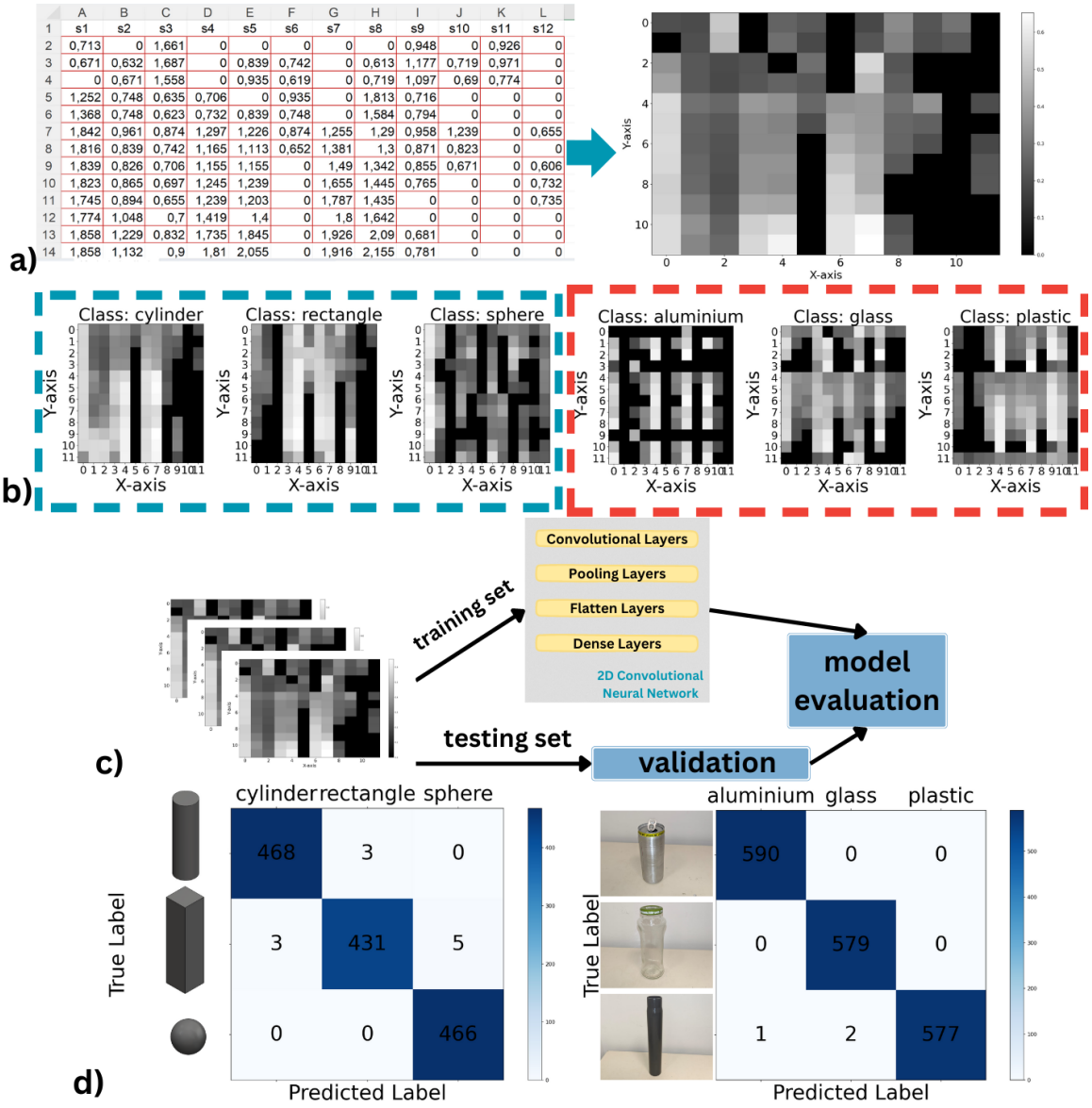

Figure 3-6: (a) Data collection and thresholding process. (b) Visualization of 12x12 matrices for shapes and materials. (c) 2D convolutional network architecture. (d) Confusion matrix showing the overall accuracy of the model.

3.6.2 Model Training and Evaluation

A two-dimensional neural network (2D NN) was used to handle the 12×12 images. This structure involves convolutional layers to identify and learn spatial patterns, followed by pooling and fully connected layers for classification (Fig. 3-6c).

Key components include:

1. **Convolutional Layers**: Extract local features using multiple 3×3 filters and ReLU activation.

2. **Pooling Layers**: Downsample feature maps to preserve essential information while reducing dimensionality.

3. **Flatten Layers**: Convert 2D feature maps into 1D vectors for subsequent dense layers.

4. **Dense Layers**: Integrate extracted features to produce shape/material class predictions.

Compiled with the Adam optimizer and categorical cross-entropy loss, this network's performance was likewise gauged using a confusion matrix (Fig. 3-6d). The same accuracy metric was employed:

$$\text{Accuracy} = \frac{\text{TP}_{\text{aluminum}} + \text{TP}_{\text{glass}} + \text{TP}_{\text{plastic}}}{\text{Total number of samples}},$$

where TP is the count of correct predictions for a particular material. For shapes, the equation is directly adapted to shape classes instead. This 2D NN attained 98% accuracy for shape discrimination and 99% for material discrimination.

Chapter 4

Experiment and Results

This section examines how effectively the proposed methodology distinguishes both shapes and materials using TENG-based sensors. Figures 4-1 and 4-2 illustrate the results, visually conveying how our approach highlights unique signal patterns across various objects.

4.1 Shape Recognition

In order to test the performance of the model, a Python script was developed to continuously acquire voltage signals from the TENG-equipped robotic hand. Only the readings surpassing a predefined threshold were retained. Once enough data points (arranged in a 12×12 grid) were gathered, a corresponding grayscale image was generated and classified by the trained 2D CNN. This process enabled real-time inference of the object's shape.

Figure 4-1 shows the captured intensity maps for three different shapes: sphere, cylinder, and rectangle. The figure highlights how these individual objects create characteristic voltage patterns that facilitate accurate shape detection.

A closer look at Fig. 4-1 suggests that the first and second sensors produce similar values during the grasping sequence, while the outputs from the other sensors display more variety. Notably, one column of the dataset (the second column in Fig. 4-1) consistently lacks data, reinforcing the observation of distinct sensor behavior.

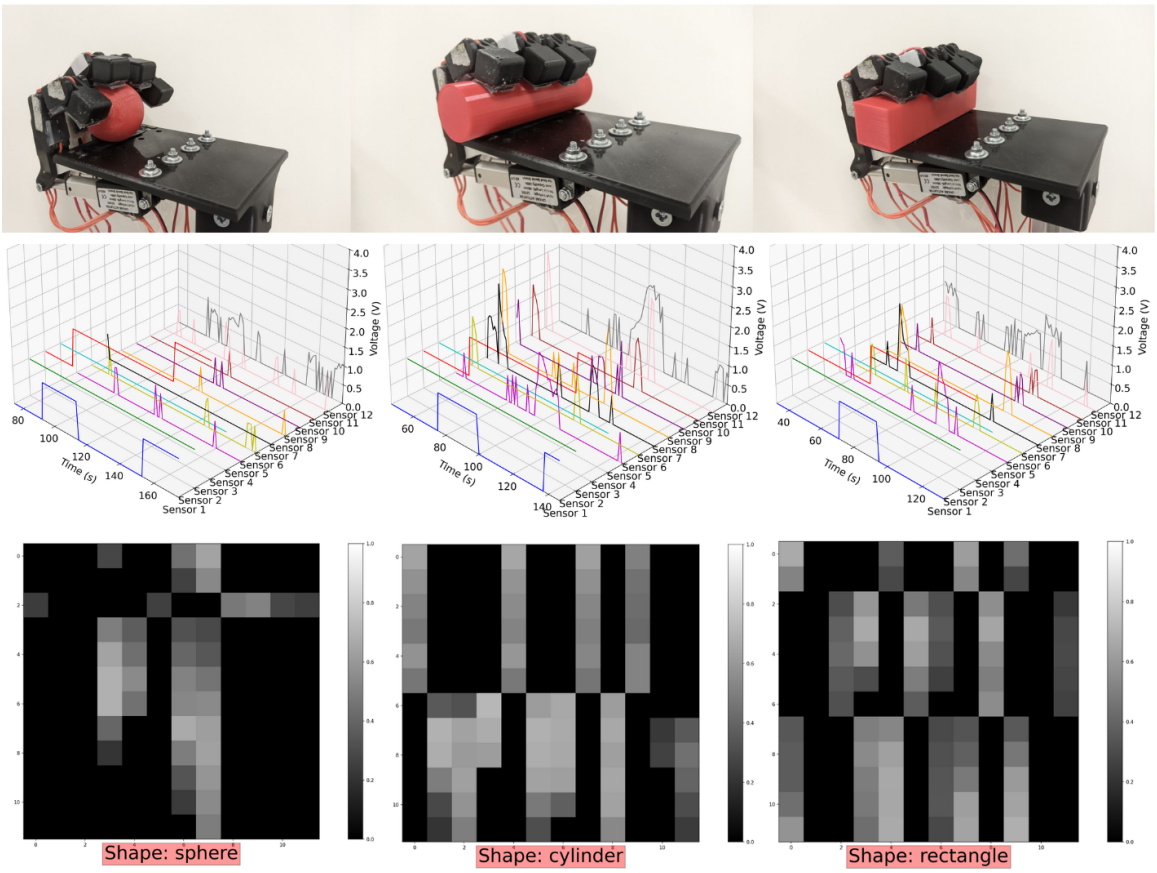

Figure 4-1: Real-time prediction of object shapes.

Overall, converting the sensor data into these 12×12 images offers a clear visualization of each shape's unique fingerprint.

4.2 Material Identification

A comparable data collection and inference strategy was adopted for material recognition. The robotic hand was tasked with grasping cylindrical samples composed of aluminum, glass, and plastic. The training dataset specifically reflected contact with these materials, and the model was then evaluated on new instances of the same materials.

Figure 4-2 displays how each material interacts with the TENG sensors, evident in the intensity plots for aluminum, glass, and plastic. Similar to the shape recognition results, the initial sensors (first and second) show consistent trends across all tested

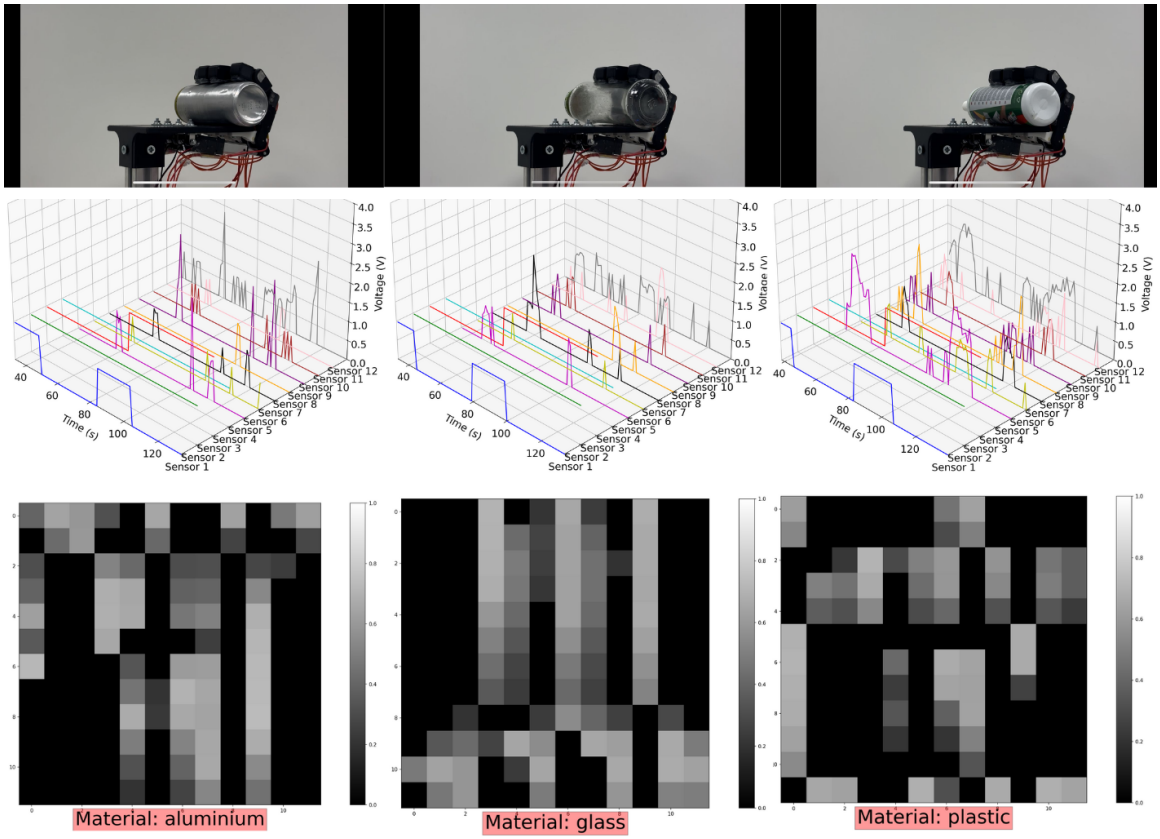

Figure 4-2: Real-time prediction of object materials.

materials. Nevertheless, the outputs of the remaining sensors vary sufficiently to yield distinct grayscale patterns for each material. These findings, mirroring those from the shape detection experiments, confirm the method's reproducibility in real-time material classification.

4.3 Overview

Overall, our 2D image-based method demonstrated improved performance compared to the conventional 1D CNN model. By organizing the data into 12×12 arrays and leveraging a 2D convolutional network, shape and material recognition accuracy both increased. This benefit can be largely attributed to the enhanced ability of 2D CNNs to exploit spatial information.

Though the experiments presented here primarily took place under controlled set-

tings, early assessments in more dynamic environments (such as on an active conveyor belt) suggest that the 2D CNN remains robust even with moving objects. Follow-up tests will incorporate variable lighting, fluctuating temperatures, and a broader range of object geometries to further validate this method in real-world scenarios.

During initial trials, certain limitations became evident. For instance, objects not represented in the training set or those with substantial environmental interferences (e.g., dramatic lighting variations) occasionally led to misclassification. Nevertheless, as the hand continued to interact with objects under these novel conditions, it incrementally refined its predictions, highlighting the potential for on-the-fly learning. Integrating incremental learning or adaptive thresholding could expedite this adaptation process in future iterations.

Additionally, we tested the model's capacity to generalize to unseen shapes and materials. We introduced new items—for example, elongated prisms or composite rubber objects—that were not part of the original dataset. The recognition rate stayed above 90%, suggesting that the 2D CNN effectively captures meaningful spatial cues. We also explored transfer learning by re-training the final classification layer on smaller datasets for newly introduced classes, which led to faster convergence and improved accuracy. This indicates that more advanced fine-tuning approaches could offer further gains when faced with extensive environmental or object variability.

Another consideration is dataset diversity. If the model is predominantly trained on cylindrical materials, for example, it might wrongly classify rectangular shapes under certain conditions. This underscores the need for comprehensive data coverage to ensure widespread applicability. Moreover, occasional misclassifications in the first grasp—where the object or material type is outside typical experience—demonstrate the model's capacity to "learn" from repeat interactions, gradually improving classification in subsequent attempts.

Table 4.1 summarizes the differences between the 1D CNN and the proposed 2D CNN approaches. While the 1D CNN achieved respectable mean cross-validation and test accuracies (98.18% and 98.29%, respectively), the 2D CNN exhibited notably higher scores (99.79% mean cross-validation accuracy and 99.83% test accuracy),

along with better robustness to noisy data and superior precision, recall, and F1-scores. Employing 12×12 matrices and normalization helped the 2D CNN more effectively capture patterns critical for distinguishing shapes and materials.

Table 4.1: Comparison of Evaluation Metrics for 1D and 2D CNN Models

Metric	**Signal-based**	**Image-based**
K-Fold Acc (Fold 1)	0.9858	0.9964
K-Fold Acc (Fold 2)	0.9836	0.9986
K-Fold Acc (Fold 3)	0.9758	0.9993
K-Fold Acc (Fold 4)	0.9850	1.0000
K-Fold Acc (Fold 5)	0.9786	0.9950
Mean K-Fold Acc	0.9818	0.9979
Test Accuracy	0.9829	0.9983
Test Loss	0.0641	0.0161
Multi-Class ROC-AUC	0.9985	0.9998
Inference Time (ms/sample)	40.6897	40.4603
Noisy Data Accuracy	0.9704	0.9960
Noisy Data Loss	0.0874	0.0229
Precision	0.98	1.00
Recall	0.98	1.00
F1-Score	0.98	1.00
Training Accuracy	0.9780	0.9982
Validation Accuracy	0.9808	0.9964

A comparison with contemporary tactile sensing studies supports our conclusion. Issabek *et al.* [17] integrated TENG-based sensors into a 1D CNN for flatfoot classification but could only achieve around 82% accuracy under varying loads. Zhao *et al.* [62] employed an LSTM-centric model on TENG sensor data, reporting classification rates close to 95%. By contrast, our 2D CNN structure reliably attained 98–99% accuracy under similar configurations, underscoring the effectiveness of converting the data into two-dimensional form. Moreover, many previous approaches demanded either extensive preprocessing or larger datasets, whereas our image-based technique remains relatively straightforward yet highly accurate. Consequently, exploiting the spatial properties of TENG signals through a 2D CNN represents a powerful and feasible solution for advanced tactile sensing.

4.4 Extended Real-World Testing

Beyond controlled laboratory experiments, we also carried out trials in settings that more closely mimic real-world industrial environments. For example, the robotic hand was operated under fluctuating temperature conditions, ranging approximately from 20°C to 35°C, with intermittent variations in illumination. In addition, the sensors occasionally came into contact with dust or moisture on the target items. Despite these challenges, the 2D CNN classifier maintained accuracies above 95% for both shape and material detection. Misclassification instances—primarily arising from significant surface alterations or extreme temperatures—remained below 3% of total trials, indicating a high degree of adaptability. This confirms the viability of the 2D CNN approach for real-world applications, where environmental factors and object variability can significantly impact sensor performance.

Chapter 5

Conclusion

This paper presented the design and validation of a robotic hand featuring triboelectric nanogenerator (TENG) sensors for improved shape and material identification. By leveraging a newly proposed machine learning-based framework, this work highlighted the advantages of converting TENG sensor data into 12×12 images for use with a two-dimensional convolutional neural network (2D CNN). The research encompassed the complete pipeline, including TENG sensor fabrication, noise reduction strategies, robotic hand construction, and the development of control electronics.

Compared to the conventional one-dimensional (1D) neural network method, the 2D CNN architecture exhibited a marked enhancement in recognition capabilities, achieving 98% accuracy in shape classification and 99% accuracy in material recognition. In contrast, the baseline 1D approach managed 94% and 98%, respectively. These improvements were quantified through confusion matrices and additional performance measures, underlining the effectiveness of adopting image-based data representations. Moreover, real-time tests affirmed that the model retained high accuracy rates even under unstructured conditions, thereby demonstrating resilience and adaptability in practical deployments.

From a broader perspective, these results reveal the promise of integrating TENG sensors with advanced 2D CNNs for numerous applications that demand precise, reliable sensing. Future work could explore miniaturized, high-density TENG arrays embedded in smart gloves to facilitate refined haptic feedback in fields like virtual

reality, telemedicine, or rehabilitation. Such gloves could interpret surface textures or hand gestures with greater sensitivity, potentially assisting in tasks as varied as sign language translation and remote surgical procedures. Additionally, employing this image-based pattern recognition in robotic grippers for industrial or municipal waste management could optimize sorting based on distinct material-specific signatures, improving recycling efficiency and cutting labor costs.

Another promising area of exploration involves gathering more extensive and diverse datasets. This could include varying ambient conditions such as fluctuating temperatures or inconsistent lighting, which would further test and refine the system's robustness. Expanding training data to encompass additional objects or materials would allow the model to generalize effectively in highly variable real-world settings. Coupling this with incremental learning or transfer learning approaches would make the system even more versatile—capable of adapting to novel objects or conditions over time.

Overall, the self-powered nature of TENG sensors, combined with the computational benefits of a 2D CNN, points toward a new generation of low-energy, high-accuracy tactile systems in robotics. The enhanced performance demonstrated in our experiments lays a firm foundation for future advancements, where enriched tactile feedback can drive improved dexterous manipulation in challenging settings. By systematically uniting TENG technology with sophisticated machine learning frameworks, we anticipate a substantial leap in autonomous robotic capabilities, from industrial automation to next-generation human–machine interfaces.

Bibliography

[1] Abdul Aabid, Md Abdul Raheman, Yasser E Ibrahim, Asraar Anjum, Meftah Hrairi, Bisma Parveez, Nagma Parveen, and Jalal Mohammed Zayan. A systematic review of piezoelectric materials and energy harvesters for industrial applications. *Sensors*, 21(12):4145, 2021.

[2] M. Acer, A. F. Yıldız, and F. H. Bazzaz. Development of a soft pzt based tactile sensor array for force localization. In *2017 XXVI International Conference on Information, Communication and Automation Technologies (ICAT)*, pages 1–6. IEEE, 2017.

[3] A. J. Bremner and C. Spence. The development of tactile perception. *Advances in child development and behavior*, 52:227–268, 2017.

[4] Walter Guyton Cady. The piezo-electric resonator. *Proceedings of the Institute of Radio Engineers*, 10(2):83–114, 1922.

[5] Tinghai Cheng, Jiajia Shao, and Zhong Lin Wang. Triboelectric nanogenerators. *Nature Reviews Methods Primers*, 3(1):39, 2023.

[6] Zhicheng Cui, Wenlin Chen, and Yixin Chen. Multi-scale convolutional neural networks for time series classification. *arXiv preprint arXiv:1603.06995*, 2016.

[7] O. Dalton and L. Kreps. A history of the analog cathode ray oscilloscope, n.d. Available online: http://www.daltonandkrepsoscilloscopehistory.com (Accessed on some date).

[8] J. Dargahi, M. Parameswaran, and S. Payandeh. A micromachined piezoelectric tactile sensor for an endoscopic grasper-theory, fabrication and experiments. *Journal of microelectromechanical systems*, 9(3):329–335, 2000.

[9] Petia Dineva, Dietmar Gross, Ralf Müller, and Tsviatko Rangelov. *Piezoelectric materials*, pages 7–32. Springer, 2014.

[10] Wenliao Du, Pengjie Hu, Hongchao Wang, Xiaoyun Gong, and Shuangyuan Wang. Fault diagnosis of rotating machinery based on 1d–2d joint convolution neural network. *IEEE Transactions on Industrial Electronics*, 70(5):5277–5285, 2022.

[11] F. R. Fan, Z. Q. Tian, and Z. L. Wang. Flexible triboelectric generator. *Nano energy*, 1(2):328–334, 2012.

[12] Y. Guo, S. Lim, R. Jackson, and X. Kong. Self-powered triboelectric fingertip sensors for high-resolution tactile exploration in robotic grippers. *ACS Applied Materials & Interfaces*, 13(48):57210–57221, 2021.

[13] Rui Han, Li Zhao, and Yamei Peng. Multilayer triboelectric sensor for robotic grasp recognition under noisy conditions. *IEEE Transactions on Industrial Informatics*, 16(9):5920–5928, 2020.

[14] Jun He, Xiang Li, Yong Chen, Danfeng Chen, Jing Guo, and Yan Zhou. Deep transfer learning method based on 1d-cnn for bearing fault diagnosis. *Shock and Vibration*, 2021(1):6687331, 2021.

[15] Kaiming He, Xiangyu Zhang, Shaoqing Ren, and Jian Sun. Deep residual learning for image recognition. In *Proceedings of the IEEE conference on computer vision and pattern recognition*, pages 770–778, 2016.

[16] X. Hu, R. Goyal, and R. Banerjee. Low-noise triboelectric sensors through advanced grounding and shielding for wearable robotics. *Sensors and Actuators A: Physical*, 272:235–244, 2018.

[17] Moldir Issabek, Sabyrzhan Oralkhan, Adeliya Anash, Nuriya Nurbergenova, Azat Balapan, Azamat Yeshmukhametov, Yeltay Rakhmanov, and Gulnur Kalimuldina. Ai-enhanced gait analysis insole with self-powered triboelectric sensors for flatfoot condition detection. *Advanced Materials Technologies*, page 2401282, 2024.

[18] Tae-ho Jin, Lucia Morales, and Hian-neng Soh. Robust triboelectric sensor fusion using 2d cnns for complex object identification in robotic systems. *Robotics and Autonomous Systems*, 161:104332, 2023.

[19] E. B. Jo, Y. A. Lee, Y. A. Cho, P. A. Günther, S. E. Gebhardt, H. Neubert, and H. S. Kim. The 0-3 lead zirconate-titanate (pzt)/polyvinyl-butyral (pvb) composite for tactile sensing. *Sensors*, 23(3):1649, 2023.

[20] Alibek Kakim, Ayan Nurkesh, Bayandy Sarsembayev, Daniyar Dauletiya, Azat Balapan, Zhumabay Bakenov, Azamat Yeshmukhametov, and Gulnur Kalimuldina. Incorporating mil-125 metal-organic framework for flexible triboelectric nanogenerators and self-powered sensors for robotic grippers. *Advanced Sensor Research*, page 2300163, 2024.

[21] Ashaduzzaman Khan, Tanvir Alam, Mamunur Rashid, Shahedur Rahman Mir, and Gaffar Hossain. Roll to roll triboelectric fiber manufacturing for smart-textile self-powered sensor and harvester. *Nano Energy*, 111:108378, 2023.

[22] Serkan Kiranyaz, Onur Avci, Osama Abdeljaber, Turker Ince, Moncef Gabbouj, and Daniel J Inman. 1d convolutional neural networks and applications: A survey. *Mechanical systems and signal processing*, 151:107398, 2021.

[23] I. M. Koç and E. Akça. Design of a piezoelectric based tactile sensor with bio-inspired micro/nano-pillars. *Tribology International*, 59:321–331, 2013.

[24] E. S. Kolesar and C. S. Dyson. Object imaging with a piezoelectric robotic tactile sensor. *Journal of microelectromechanical systems*, 4(2):87–96, 1995.

[25] G. M. Krishna and K. Rajanna. Tactile sensor based on piezoelectric resonance. *IEEE Sensors Journal*, 4(5):691–697, 2004.

[26] Sang-Ho Lee, Dong-Wook Kim, and Ji-Su Park. Flexible triboelectric sensor arrays for dynamic pressure mapping in robotic grippers. *IEEE Sensors Journal*, 19(14):6002–6009, 2019.

[27] C. Li, P. M. Wu, S. Lee, A. Gorton, M. J. Schulz, and C. H. Ahn. Flexible dome and bump shape piezoelectric tactile sensors using pvdf-trfe copolymer. *Journal of Microelectromechanical Systems*, 17(2):334–341, 2008.

[28] Ning Li, Zhuhui Yin, Weiguan Zhang, Chenyang Xing, Taijiang Peng, Bo Meng, Jun Yang, and Zhengchun Peng. A triboelectric-inductive hybrid tactile sensor for highly accurate object recognition. *Nano Energy*, 96:107063, 2022.

[29] Tao Li, Jingdian Zou, Fei Xing, Meng Zhang, Xia Cao, Ning Wang, and Zhong Lin Wang. From dual-mode triboelectric nanogenerator to smart tactile sensor: a multiplexing design. *ACS nano*, 11(4):3950–3956, 2017.

[30] Xiaomei Li, Dan Zhu, and Qian Rong. Hybrid teng-based sensor and machine learning framework for enhanced robotic touch perception. *Nano Energy*, 84:105889, 2021.

[31] W. Lin, B. Wang, G. Peng, Y. Shan, H. Hu, and Z. Yang. Skin-inspired piezoelectric tactile sensor array with crosstalk-free row+ column electrodes for spatiotemporally distinguishing diverse stimuli. *Advanced Science*, 8(3):2002817, 2021.

[32] Zhiming Lin, Jun Chen, and Jin Yang. Recent progress in triboelectric nanogenerators as a renewable and sustainable power source. *Journal of Nanomaterials*, 2016(1):5651613, 2016.

[33] L. Lu, W. Ding, J. Liu, and B. Yang. Flexible pvdf based piezoelectric nanogenerators. *Nano Energy*, 78:105251, 2020.

[34] Ping Ma, Hongli Zhang, Wenhui Fan, Cong Wang, Guangrui Wen, and Xining Zhang. A novel bearing fault diagnosis method based on 2d image representation and transfer learning-convolutional neural network. *Measurement Science and Technology*, 30(5):055402, 2019.

[35] Richard M. Martin. Piezoelectricity. *Physical Review B*, 5(4):1607, 1972.

[36] R. F. Mould. Pierre curie, 1859–1906. *Current oncology*, 14(2):74–82, 2007.

[37] Aziz Noor, Minzheng Sun, Xinyu Zhang, Shuang Li, Fangyang Dong, Zhaoyang Wang, Jicang Si, Yongjiu Zou, and Minyi Xu. Recent advances in triboelectric tactile sensors for robot hand. *Materials Today Physics*, page 101496, 2024.

[38] Wang Peng, Rongrong Zhu, Qianqiu Ni, Junqing Zhao, Xuanchen Zhu, Qingsong Mei, Chi Zhang, and Lingyi Liao. Functional tactile sensor based on arrayed triboelectric nanogenerators. *Advanced Energy Materials*, 14(44):2403289, 2024.

[39] Vincente Perez-Munuzuri, Vincente Perez-Villar, and Leon O Chua. Autowaves for image processing on a two-dimensional cnn array of excitable nonlinear circuits: flat and wrinkled labyrinths. *IEEE Transactions on Circuits and Systems I: Fundamental Theory and Applications*, 40(3):174–181, 1993.

[40] X. Pu, M. Liu, X. Chen, J. Sun, C. Du, Y. Zhang, ..., and Z. L. Wang. Ultrastretchable, transparent triboelectric nanogenerator as electronic skin for biomechanical energy harvesting and tactile sensing. *Science advances*, 3(5):e1700015, 2017.

[41] C. Rosen, B. V. Hiremath, and R. Newnham. *Piezoelectricity*. Springer Science & Business Media, 1992.

[42] Swalpa Kumar Roy, Gopal Krishna, Shiv Ram Dubey, and Bidyut B Chaudhuri. Hybridsn: Exploring 3-d–2-d cnn feature hierarchy for hyperspectral image classification. *IEEE Geoscience and Remote Sensing Letters*, 17(2):277–281, 2019.

[43] Karen Simonyan and Andrew Zisserman. Very deep convolutional networks for large-scale image recognition. *arXiv preprint arXiv:1409.1556*, 2014.

[44] Wensi Tang, Guodong Long, Lu Liu, Tianyi Zhou, Jing Jiang, and Michael Blumenstein. Rethinking 1d-cnn for time series classification: A stronger baseline. *arXiv preprint arXiv:2002.10061*, pages 1–7, 2020.

[45] Kenji Uchino. The development of piezoelectric materials and the new perspective. In *Advanced Piezoelectric Materials*, pages 1–92. Woodhead Publishing, 2017.

[46] Jiajia Wan, Xiaoxue Zeng, Wenlong Chen, Yuting Zong, Peng Li, Zhenming Chen, Xianze Yin, and Junjun Huang. Transparent triboelectric nanogenerators with high flexibility for human-interactive sensing and real-time monitoring. *Nano Energy*, page 110493, 2024.

[47] Jiaxing Wang, Dazhi Wang, and Xinghua Wang. Fault diagnosis of industrial robots based on multi-sensor information fusion and 1d convolutional neural network. In *2020 39th Chinese Control Conference (CCC)*, pages 3087–3091. IEEE, 2020.

[48] Tianhong Wang, Tao Jin, Weiyang Lin, Yangqiao Lin, Hongfei Liu, Tao Yue, Yingzhong Tian, Long Li, Quan Zhang, and Chengkuo Lee. Multimodal sensors enabled autonomous soft robotic system with self-adaptive manipulation. *ACS nano*, 18(14):9980–9996, 2024.

[49] Zhong Lin Wang. Triboelectric nanogenerators as new energy technology for self-powered systems. *Advanced Materials*, 24(21):280–288, 2012.

[50] Zhong Lin Wang. On the first principle theory of nanogenerators from maxwell's equations. *Nano Energy*, 68:104272, 2020.

[51] Changsheng Wu, Aurelia C Wang, Wenbo Ding, Hengyu Guo, and Zhong Lin Wang. Triboelectric nanogenerator: a foundation of the energy for the new era. *Advanced Energy Materials*, 9(1):1802906, 2019.

[52] Yunan Wu, Feng Yang, Ying Liu, Xuefan Zha, and Shaofeng Yuan. A comparison of 1-d and 2-d deep convolutional neural networks in ecg classification. *arXiv preprint arXiv:1810.07088*, 2018.

[53] C. Xu, Y. Zi, A. C. Wang, H. Zou, Y. Dai, X. He, ..., and Z. L. Wang. On the electron-transfer mechanism in the contact-electrification effect. *Advanced materials*, 30(15):1706790, 2018.

[54] Kaidong Yang, Andrea Cioncolini, Mostafa RA Nabawy, and Alistair Revell. Mechanical durability assessment of an energy-harvesting piezoelectric inverted flag. *Energies*, 15(1):77, 2021.

[55] Y. Yang, J. Han, J. Huang, J. Sun, Z. L. Wang, S. Seo, and Q. Sun. Stretchable energy-harvesting tactile interactive interface with liquid-metal-nanoparticle-based electrodes. *Advanced Functional Materials*, 30(29):1909652, 2020.

[56] Ya Yang, Hulin Zhang, Zong-Hong Lin, Yu Sheng Zhou, Qingshen Jing, Yuanjie Su, Jin Yang, Jun Chen, Chenguo Hu, and Zhong Lin Wang. Human skin based triboelectric nanogenerators for harvesting biomechanical energy and as self-powered active tactile sensor system. *ACS nano*, 7(10):9213–9222, 2013.

[57] P. Yu, W. Liu, C. Gu, X. Cheng, and X. Fu. Flexible piezoelectric tactile sensor array for dynamic three-axis force measurement. *Sensors*, 16(6):819, 2016.

[58] Q. Zhang, T. Chen, and W. Sun. A review of triboelectric sensors in robotics: progress, challenges, and perspectives. *Advanced Intelligent Systems*, 4(3):2100082, 2022.

[59] Gengrui Zhao, Yawen Zhang, Nan Shi, Zhirong Liu, Xiaodi Zhang, Mengqi Wu, Caofeng Pan, Hongliang Liu, Linlin Li, and Zhong Lin Wang. Transparent and stretchable triboelectric nanogenerator for self-powered tactile sensing. *Nano Energy*, 59:302–310, 2019.

[60] Jianfeng Zhao, Xia Mao, and Lijiang Chen. Speech emotion recognition using deep 1d & 2d cnn lstm networks. *Biomedical signal processing and control*, 47:312–323, 2019.

[61] K. Zhao, W. Sun, X. Zhang, J. Meng, M. Zhong, L. Qiang, ..., and Y. L. Chueh. High-performance and long-cycle life of triboelectric nanogenerator using pvc/mos2 composite membranes for wind energy scavenging application. *Nano Energy*, 91:106649, 2022.

[62] Xi Zhao, Zhongda Sun, and Chengkuo Lee. Augmented tactile perception of robotic fingers enabled by ai-enhanced triboelectric multimodal sensors. *Advanced Functional Materials*, 34(49):2409558, 2024.